BAMBI – A transient 2D-MESFET model with general boundary conditions including Schottky and current controlled contacts

W. Kausel
Institut für Allgemeine Electrotechnik und Elektronik, Dept. for Physical Electronics, Technical University of Vienna, Gußhausstraße 27-29, A-1040 Vienna, Austria and Ludwig Boltzmann-Institut für Festkörperphysik

J.O. Nylander
Electronics Group, Dept. of Technology, Uppsala University, Box 534, S-751 21 Uppsala, Sweden

G. Nanz and S. Selberherr
Institut for Microelectronics, Technical University of Vienna, Gußhausstraße 27-29, A-1040 Vienna, Austria

H. Poetzl
Institut für Allgemeine Electrotechnik und Elektronik, Dept. for Physical Electronics, Technical University of Vienna, Gußhausstraße 27-29, A-1040 Vienna, Austria and Ludwig Boltzmann-Institut für Festkörperphysik

Boundary conditions using a current-dependent carrier recombination velocity distribution are developed for modelling Schottky contacts by computer-aided physical simulation. In addition, a boundary condition in the form of an abitrary linear combination of voltage and current at the contact is presented. Thus MESFET devices with simple circuits connected to device terminals can be simulated by solving additional equations. As an example the switching behaviour of a MESFET with a drain resistor is investigated.

1. Introduction

MESFETs are a potential alternative to MOSFETs. MESFETs offer advantages in terms of simplicity of fabrication compared with MOSFETs, because only low-temperature processes are required for fabrication. Without any radiation-sensitive oxide under the gate MESFETs have been reported to stand up to 100 Mrad [1] compared to values of a few hundred krad for MOSFETs. In the MOS case, hot carriers may be injected into the oxide. This fixed charge causes degradation of the characteristics. The effective mobility in the channel also tends to be higher in the MES case. The current flows further inside the silicon, causing less

interaction between carriers and the interface states. MESFETs therefore show little noise, being similar to JFETs in this respect. Due to these advantages, concepts for complementary silicon MESFETs have been investigated as an alternative to the traditional CMOS technology [2].

Such investigations urgently require the help of device simulation tools with adequate models for ohmic and Schottky contacts. This paper presents the implementation of boundary conditions for metal–semiconductor contacts and for floating contacts in the two-dimensional transient device simulator BAMBI [3,4]. The program simulates devices with arbitrary geometry and doping profile. It solves the three basic semiconductor equations (1–3) according to drift diffusion theory [5], together with two current equations (4, 5) using the method of finite boxes [6]: boxes [6]:

$$\Delta\psi = -\frac{q}{\varepsilon}(p-n+N_D-N_A) \tag{1}$$

$$\nabla J_n = q(\frac{\partial n}{\partial t} + R_n) \tag{2}$$

$$\nabla J_p = -q(\frac{\partial p}{\partial t} + R_p) \tag{3}$$

$$J_n = qD_n\,\nabla n - q\mu n\nabla\psi \tag{4}$$

$$J_p = -qD_p\,\nabla p - q\mu p\nabla\psi \tag{5}$$

2. The ohmic contact

The analysis is based on the presumption that the electrostatic potential and electron and hole concentrations (ψ,n,p) are unknowns. Poisson's equation (1) and the two continuity equations (2, 3) are numerically solved with a Dirichlet boundary condition for electrons, holes, and electrostatic potential at ohmic contacts. Assuming space charge neutrality directly under the terminal, the concentrations are set equal to their thermal equilibrium values. The boundary condition for the electrostatic potential is

$$V_{term} = \psi - \psi_{bi} \tag{6}$$

$$\psi_{bi} = \pm\frac{kT}{q}\ln\left(\frac{|N_D - N_A|}{n_i}\right) \tag{7}$$

where ψ_{bi} denotes the built-in potential and V_{term} the terminal voltage. Simulating contacts with external circuits, V_{term} becomes floating, increasing the number of

variables to be calculated by one per floating contact. The additional equations are given by the nex mixed boundary condition (eqn. 8) defining the dependence between contact voltage V_{term} and contact current I_{term}:

$$\alpha \cdot V_{term} + \beta \cdot \left(I_{term} + C\frac{dV_{term}}{dt} \right) = \gamma \tag{8}$$

This is the most general form of the boundary condition which can be handled by our method. Thus a variety of possibilities for interpretation, in mathematical as well as in electrical terms, is offered. Choosing the appropriate dimensions of α, β and γ, several different definitions of the outer circuit diagram can be given using arbitrarily a serial resistive, or a parallel conductive and serial or parallel capacitive loads.

A current-driven circuit shown in Fig. 1 (left side), is described by defining $\alpha = G, \beta = 1, \gamma = I_{appl}$. The equivalent voltage-driven circuit diagram of Fig. 1 (centre) requires the assumption that $\alpha = 1, \beta = R$ and $\gamma = V_{appl.}$

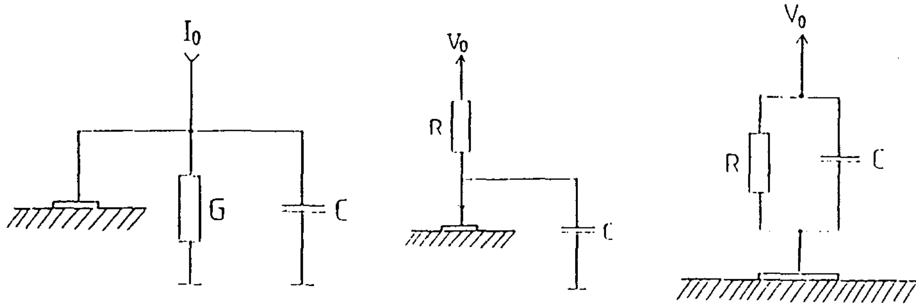

Fig. 1 Equivalent circuit diagrams

Interpreting C as a capacity between voltage source and contact, eqn. (8) has to be slightly modified by the transformation of γ: $\gamma \rightarrow \gamma + \beta\ C\frac{d(\gamma/\alpha)}{dt}$. For simpler handling by the user, eqn. (9) has been implemented directly:

$$\alpha \cdot V_{term} + \beta \cdot \left[I_{term} - C\frac{d\,(\gamma/\alpha - V_{term})}{dt} \right] = \gamma \tag{9}$$

With the values given above the outer right circuit of Fig. 1 can be simulated:

$$I_{term} = \frac{V_{appl} - V_{term}}{R} + C\frac{d(V_{appl} - V_{term})}{dt} \tag{10}$$

The numerical treatment of mixed boundary conditions, eqns. (8) or (9), is illustrated by Fig. 2. Both equations include the two variables V_{term} and I_{term}. V_{term} is the additional unknown and I_{term} has to be expressed by ψ_k, n_k, and p_k, the electrostatic potential, the electron and the hole concentration at mesh points that lie at the con-

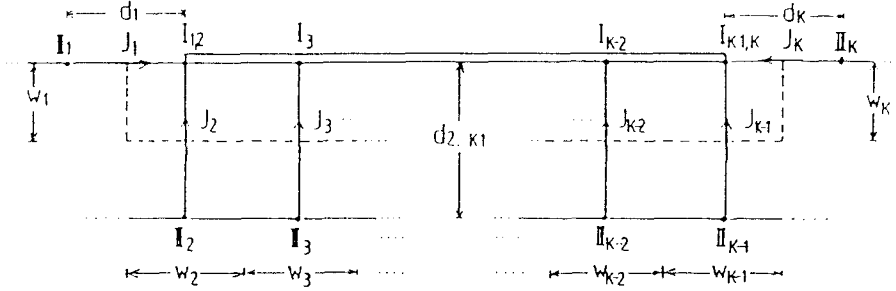

Fig. 2 Discretization of the Boundary Condition

tact or are neighbours of a contact point. The terminal current is given by integrating electron, hole and displacement current densities J_n, J_p and J_d over the area of the contact A:

$$I_{term} = \int_A (J_n + J_p + J_d) \cdot dA \tag{11}$$

Using the well known finite difference scheme first suggested by Scharfetter and Gummel [7] the boundary conditions, eqns. (8) and (9) finally yield the discrete expressions:

$$\alpha \cdot V_{term_T} + \beta \cdot \left(\sum_k (J_{n_k} + J_{p_k} + J_{d_k}) + C \frac{V_{term_T} - V_{term_{-\Delta T}}}{\Delta T} \right) = \gamma \tag{12}$$

$$\alpha \cdot V_{term_T} + \beta \cdot \left(\sum_k (J_{n_k} + J_{p_k} + J_{d_k}) - C \frac{[(\frac{\gamma}{\alpha})_T - (\frac{\gamma}{\alpha})_{T-\Delta T}] - [V_{term_T - \Delta T}]}{\Delta T} \right) = \gamma \tag{13}$$

with

$$J_{n_k} = qD_n \frac{w_k}{d_k} [n_{II_k} B(\Delta_k) - n_{I_k} B(-\Delta_k)] \tag{14}$$

$$J_{p_k} = qD_p \frac{w_k}{d_k} [p_{I_k} B(\Delta_k) - p_{II_k} B(-\Delta_k)] \tag{15}$$

$$J_{d_k} = - \frac{w_k}{d_k} \cdot \varepsilon \frac{(\psi_{II_k} - \psi_{I_k})_T - (\psi_{II_k} - \psi_{I_k})_{T-\Delta T}}{\Delta T} \tag{16}$$

$$\Delta_k = \frac{\psi_{II_k} - \psi_{I_k}}{V_T}, \qquad B(x) = \frac{x}{e^x - 1} \tag{17, 18}$$

where I denotes the point at the contact and II the next neighbour (Fig. 2). $J_{n,p,d}$ denote the three current contributions at the midpoints, T the actual time, ΔT the actual time step, d_k the distance between point I and point II and w_k the weighting factor for the integration. D_n and D_p are the coefficients for electron and hole diffusion, ε is the dielectric permittivity, q the electronic charge and V_t the thermal voltage.

Solving the discrete form of the mixed boundary condition, eqns. (11) and (12), together with a discrete representation of Poisson's equation and both continuity equations (2,3) yields a numerical solution for electrostatic potential, electron and hole concentration ψ_k, n_k, p_k at each free node in a finite-boxes mesh and the terminal voltage V_{term} for each floating contact. Since eqns. (14) and (15) are non-linear in the unknown variable V_{term} a linearization technique is required. For current or mixed boundary problems the discretized non-linear equation system is therefore solved simultaneously by a coupled Newton's method.

3. The Schottky contact

When metal is in contact with a semiconductor, potential barriers Φ_{bn} for electrons and Φ_{bp} for holes will be formed at the metal-semiconductor (MS) interface (Fig. 3). The Fermi levels in the two materials must coincide with what causes a depletion layer similar to that of the one-sided abrupt (e.g. p^+-n) junction. According to the thermionic emission-diffusion theory of Crowell and Sze [8] the boundary conditions at the MS interface read:

$$\psi_i = V_{app} - \psi_s \tag{19}$$

$$J_n = -q \cdot v_n \cdot (n_i - n_0) \tag{20}$$

$$J_p = q \cdot v_p \cdot (p_i - p_0) \tag{21}$$

n_i and p_i are the surface concentrations of electrons and holes, ψ_i the surface potential at the MS interface, V_{app} the applied voltage and ψ_{bi} the doping-dependent built-in voltage, eqn. (7).

Equation (18) defines the surface potential with the help of the barrier dependent potential value ψ_s (Fig. 4) according to the potential variation within the depletion

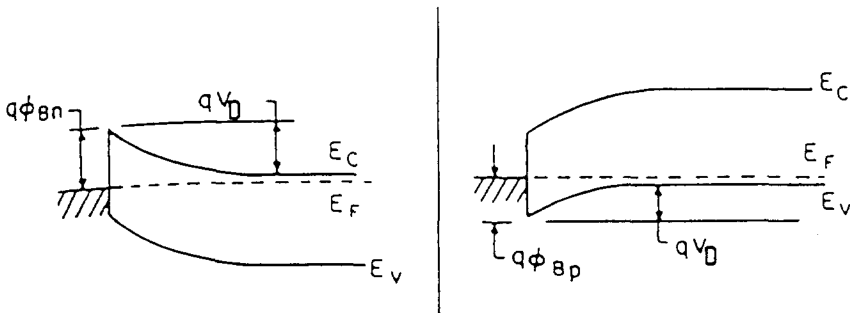

Fig. 3 Diagram of the energy bands at a Schottky contact

layer. ψ_s is defined eqns. (22, 23) by

$$\psi_s = \Phi_{bn} - \Phi_i \tag{22}$$

$$\psi_s = \Phi_i - \Phi_{bp} \tag{23}$$

where Φ_i is the intrinsic energy level.

The boundary conditions, eqns. (20) and (21) model the carrier flow through the MS interface with surface recombination terms using effective surface recombination velocities v_n and v_p for electrons and holes, respectively [9].

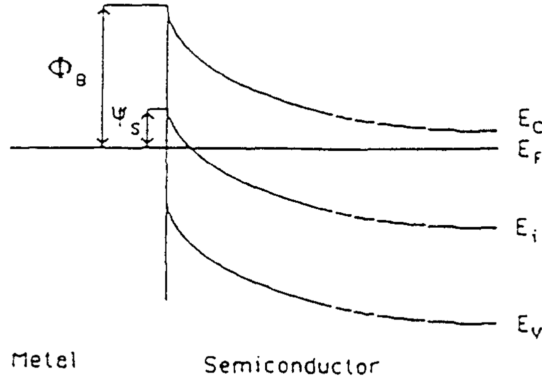

Fig. 4 Definition of the surface potential

The quasi-equilibrium concentrations n_0 and p_0 are the surface concentration for zero bias ($V_{appl} = 0$). With eqn. (19) the surface potential ψ_i becomes $\psi_i = \psi_s$ yielding

$$n_0 = n_i \cdot \exp\left(\frac{-\psi_s}{V_T}\right) \tag{24}$$

$$p_0 = n_i \cdot \exp\left(\frac{-\psi_s}{V_T}\right) \tag{25}$$

where n_i denotes the intrinsic concentration.

The recombination velocities $v_{n,p}$ at a MS junction are upper-bounded by the saturation velocities of the carriers within the semi-conductor and lower-bounded by the collection velocity v_c eqn. (26). The value of v_c has been derived by Crowell and Sze [8], assuming a Maxwellian distribution of carrier velocities at the contact:

$$v_c \big|_{(V_{appl}<0)} = \left(\frac{kT}{2m^*\pi}\right)^{1/2} \cdot f_b f_q \tag{26}$$

m^* is the effective mass for electrons or holes, f_b is the probability of a carrier reaching the metal without being back-scattered and f_q is the probability of quantum mechanical reflection of carriers together with tunnelling effects.

Defining $v_{n,p}$ equal to a fraction of v_{sat} under forward bias conditions causes unrealistic accumulation of carriers at the MS interface. Setting $v_{n,p} = v_{sat}$ in order to avoid this accumulation for high forward bias will result in an unrealistic depletion of carriers at the contact if zero or low bias is applied. As pointed out by Adams [10] one expects a non-Maxwellian distribution of velocities of carriers travelling into the metal.

Our investigations followed the approach by Adams [10], who assumed the carrier velocities to be represented by the positive part of a drifted Maxwellian distribution:

$$f(v_x) = K \cdot \exp\left(\frac{-m^*_{n,p}\gamma_{n,p}(v_x - v_d)^2}{2kT}\right) \tag{27}$$

Taking the mean value:

$$v_{n,p} = \frac{\int_0^\infty v_x f(v_x)dv_x}{\int_0^\infty f(v_x)dv_x} \tag{28}$$

yields the current-dependent expression:

$$v_{n,p} = v_d + \left(\frac{2kT}{\pi m^*_{n,p}\gamma_{n,p}}\right)^{1/2} \cdot \frac{\exp\left(-v_d^2 \cdot \frac{m^*_{n,p}\gamma_{n,p}}{2kT}\right)}{1 + \operatorname{erf}\left[v_d \cdot \left(\frac{m^*_{n,p}\gamma_{n,p}}{2kT}\right)^{1/2}\right]} \tag{29}$$

Here $v_d = \frac{J_{n,p}}{q \cdot (n,p)}$ is the drift velocity, $\gamma_{n,p}$ is a compensating factor for the increase of the carrier effective mass caused by band structure changes at the MS interface (Stratton [11]), and K is a normalization constant.

Figure 5 shows the recombination vs. drift velocity. Under reverse bias, $v_{n,p}$ are kept constant by neglecting their reduction f_b and f_q.

Equation (29) is valid in all practical cases. Since the drift velocity is upper-bounded by the saturation velocity in the semiconductor eqn. (28) is upper bounded as well. Comparing the lower bound of eqn (29) for $V_{app} = 0$ with the expression for the collection velocity yields the fitting parameter $\gamma_{n,p} = 4$. Physically this would predict a ratio $\frac{T}{m^*_{n,p}}$ at the MS interface of 0.25 times the ratio within the semiconductor.

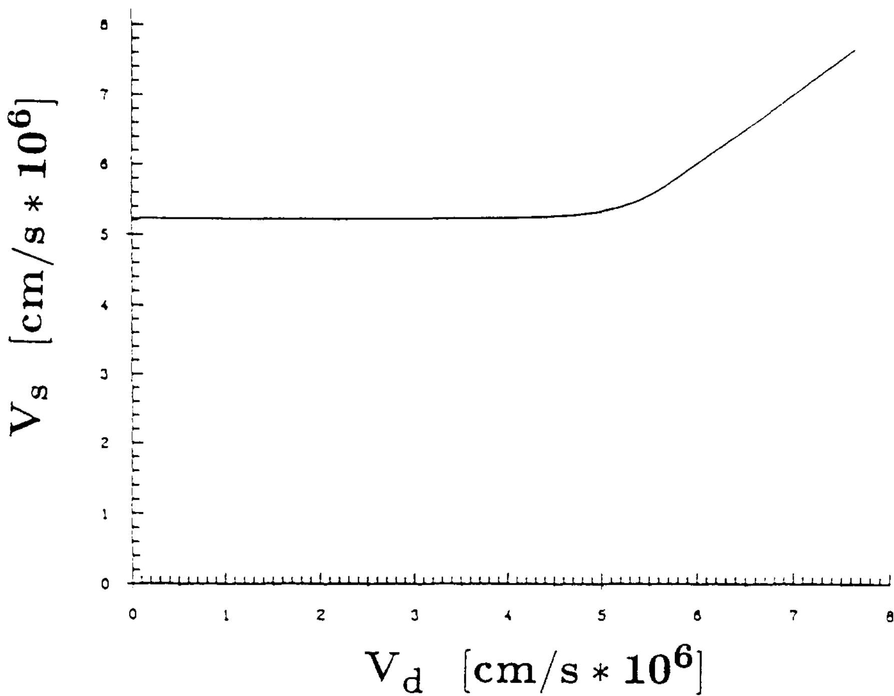

Fig. 5 Recombination velocity vs. drift velocity

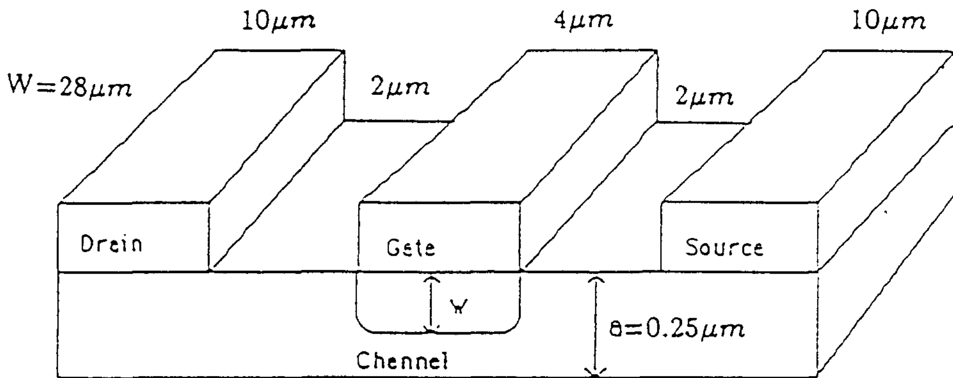

Fig. 6 Geometry of the simulated MESFET

4. Application example

As a major application the switching behaviour of an n-channel silicon MESFET with a barrier height of Φ_{bn} = 0.85 eV is presented. Figure 6 shows the geometry and Fig. 7 the simulated circuit. The gate voltage is switched abruptly from a turn-off voltage $V_{GS} = -2$ V to a turn-on voltage $V_{GS} = +0.2$ V and back to $V_{GS} = -2$ V.

4.1 Turn-on behaviour

The big voltage jump is transmitted to the drain terminal (Fig. 9) resulting in a drain voltage peak of V_{DS} = 6.78 V which is at least higher than the supply voltage. The drain current therefore flows out of the device first (Fig. 9). It changes its sign after t = 40 ps corresponding to the decreasing drain voltage which reaches the value of the supply voltage at the same time. Thus, during the first 40 ps, the current enters the device through the gate terminal; passes the depletion region as displacement current and continues as electron convection current to both the drain and the source contact. Source and gate current show significantly higher peaks since the drain current is limited by the drain resistor. Forty picoseconds after the gate voltage plus conductivity is reached in the channel region and the current starts to pass from drain to source.

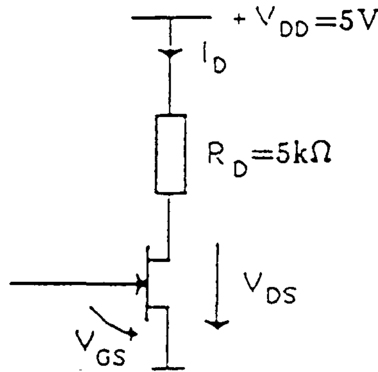

Fig. 7 Simulated circuit

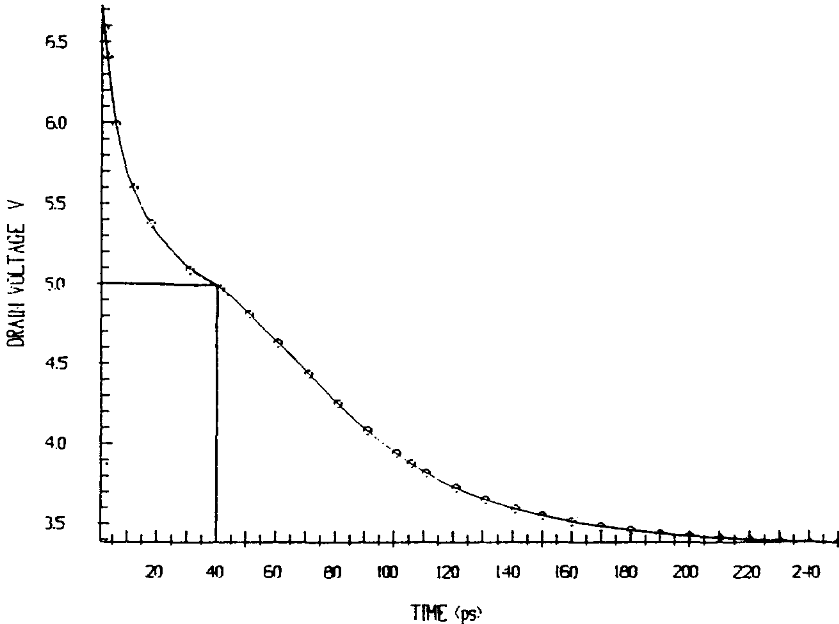

Fig. 8 Drain voltage during turn on

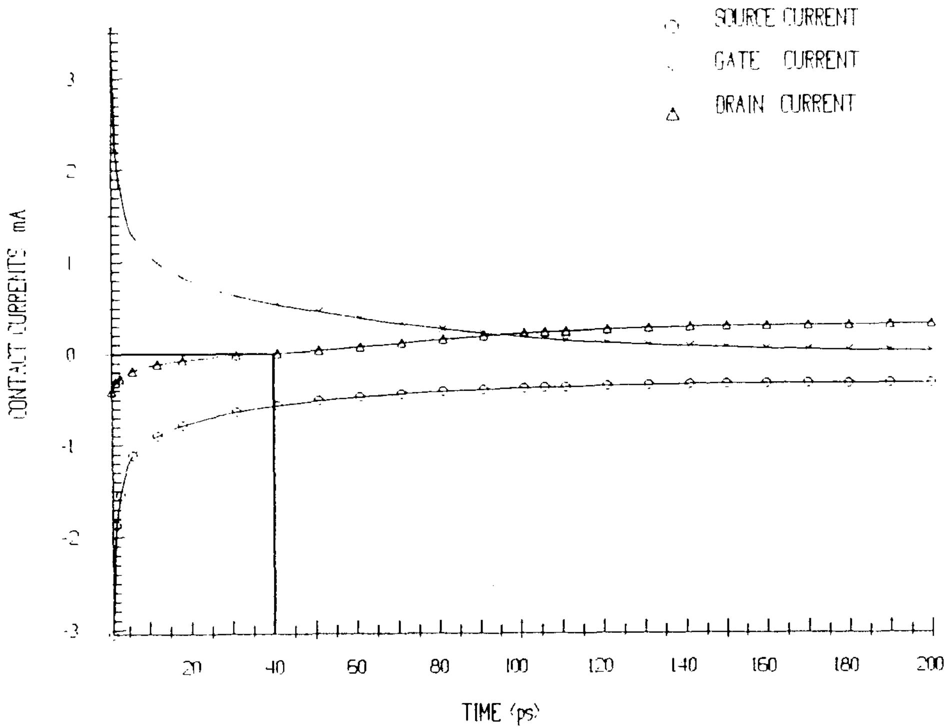

Fig. 9 Contact currents during turn on

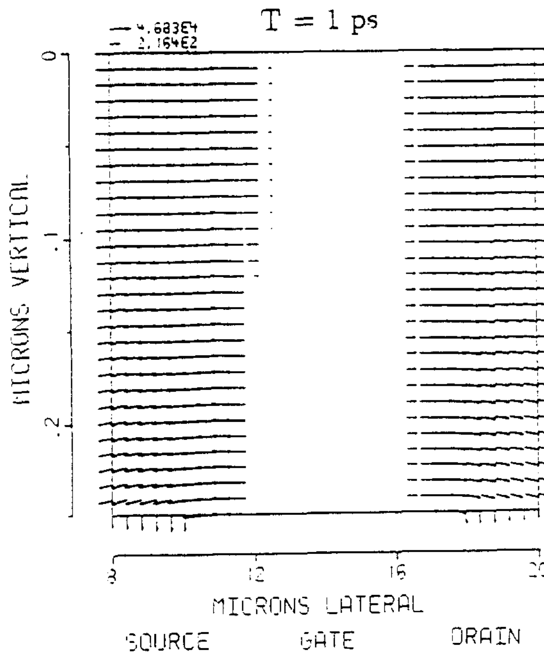

Fig. 10 Direction of the electron current density under the MES gate after 1 ps (logarithmic scale)

Figures 10 and 11 show the convection current flow under the gate metal. Electrons are flowing into the depleted region under the MES gate (Fig. 10) from both sides but the flow from the source side is obviously dominating (Figs. 9 and 10). Forty picoseconds later the drain current becomes zero and finally changes its direction (Fig. 11). In steady-state condition (Fig. 12) we observe a broad current pass at that side of the device opposite the MES gate.

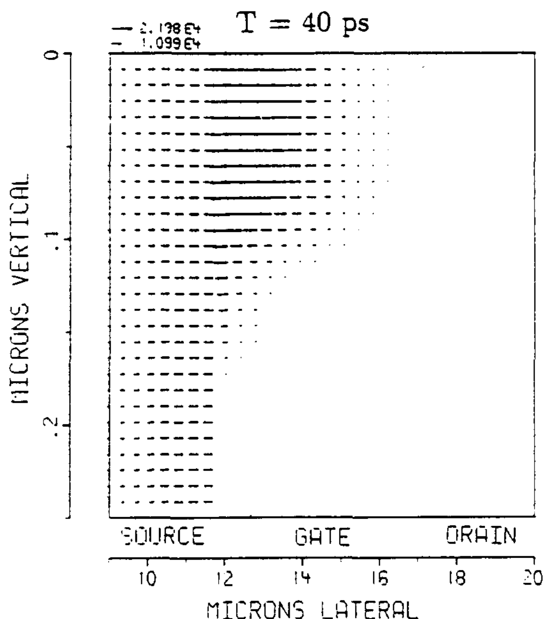

Fig. 11 Direction of the electron current density under the MES gate after 40 ps

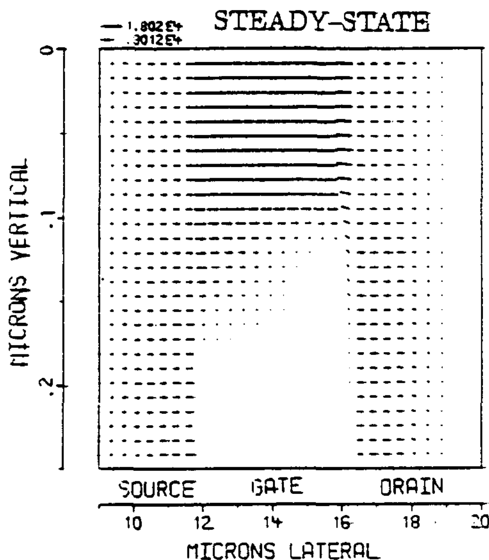

Fig. 12 Direction of the electron current density under the MES gate in steady-state condition

The build up of the channel is illustrated most efficiently with the figures of the electron distribution (Figs. 13–16). Starting with a completely depleted channel region (Fig. 13) we observe significant electron injection after 12 ps (Fig. 14). After

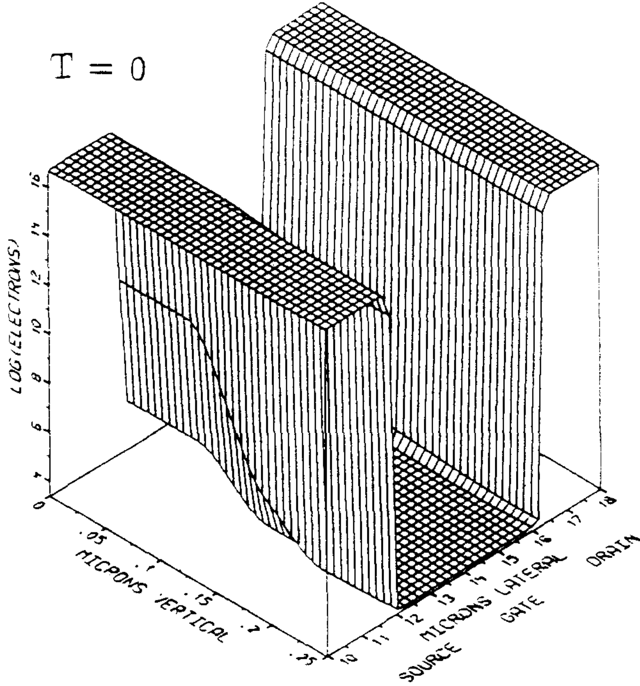

Fig. 13 Electron distribution in the channel region before turn on

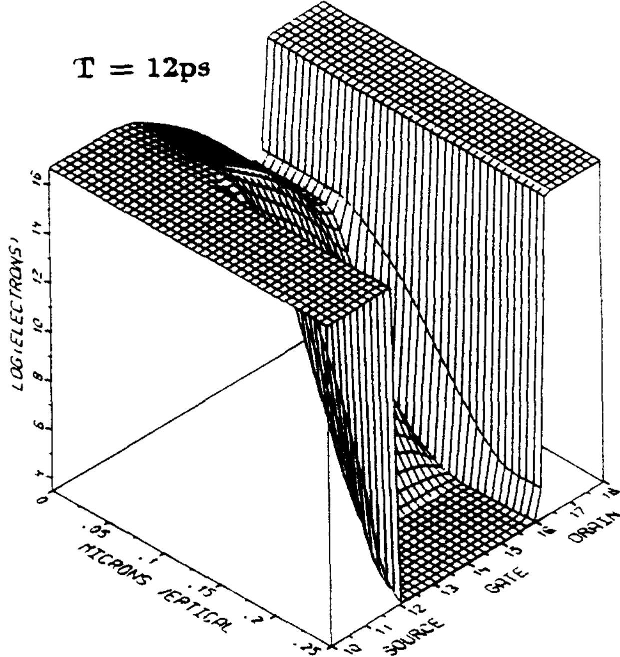

Fig. 14 Electron distribution in the channel region after 12 ps

40 ps the depletion region is reduced so far that an electron convection can start to flow directly from drain to source as mentioned above although the figure shows a small pinch off at the drain side of the channel region (Fig. 15). This pinch off is further decreased but it still exists in steady-state condition (Fig. 16). The gate-drain

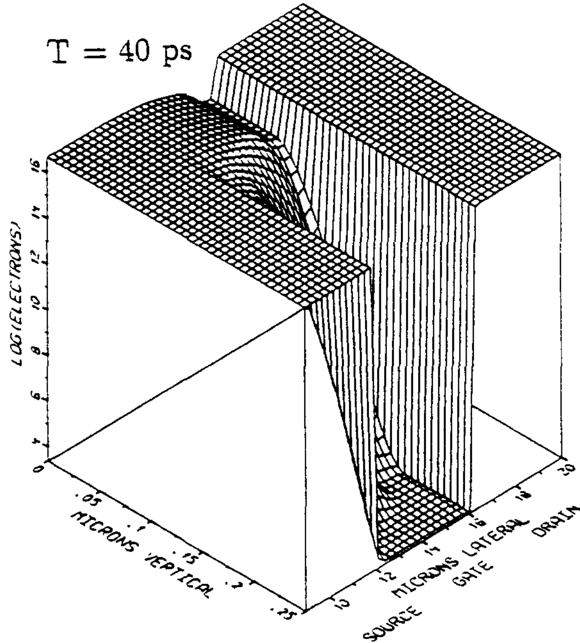

Fig. 15 Electron distribution in the channel region after 40 ps

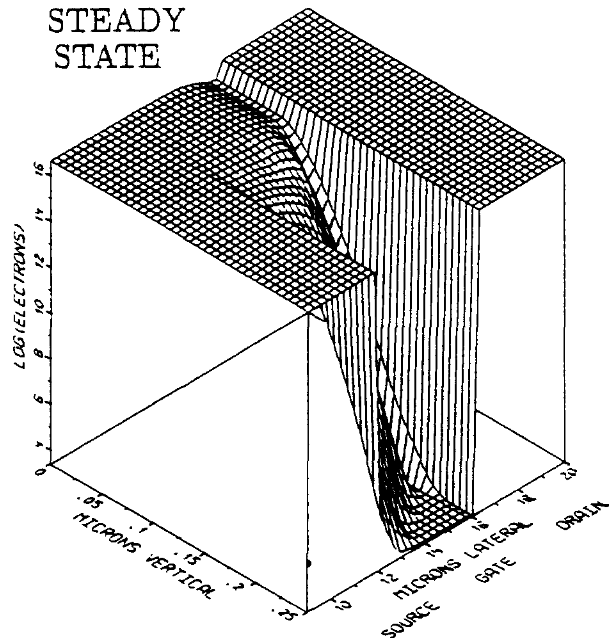

Fig. 16 Electron distribution in the channel region in steady-state condition

Schottky diode is in fact reverse biased at a drain-source voltage of V_{DS} = 3.36 V. This also is proved with the figure of the steady-state potential distribution that shows the higher potential drop at the drain side of the channel region (Fig. 17) corresponding to the higher lateral field (Fig. 18). Thus, the device is switched to a bias point in the saturation region of the output characteristic.

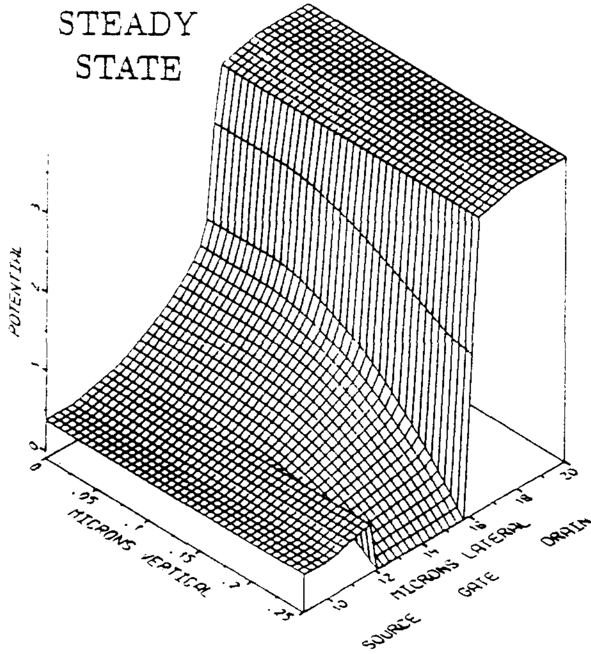

Fig. 17 Potential distribition in the channel region in steady-state condition

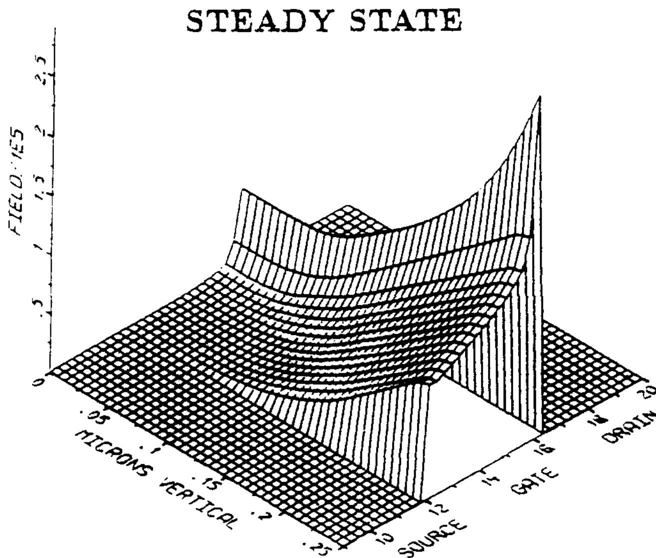

Fig. 18 Modulus of the electric field in the channel region in steady-state condition

4.2 Turn-off behaviour

The gate voltage pulse from $V_{GS} = +0.2$ V down to $V_{GS} = -2$ V is again transmitted to the drain contact. The drain voltage V_{DS} capacitively jumps from $V_{DS} = 3.36$ V down to $V_{DS} = 1.514$ V (Fig. 19). Corresponding to the higher voltage drop at the

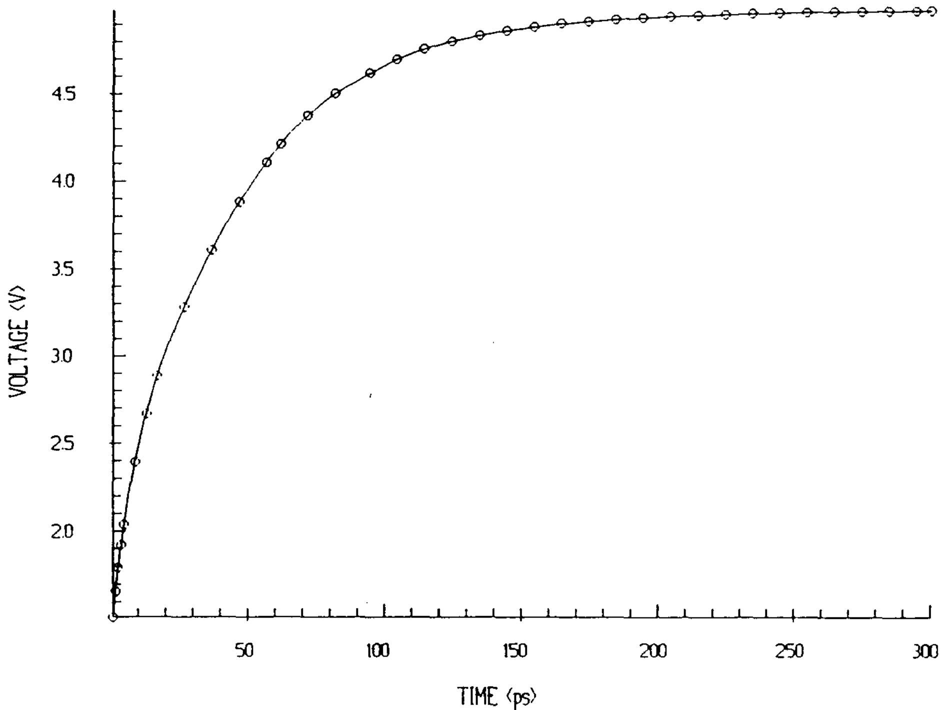

Fig. 19 Drain voltage during turn off

drain resistor, the drain current is increased to $I_D = 0.7$ mA (Fig. 20). In contrast to the turn-on case the current now enters the device through both source and drain contact and leaves through the gate terminal. Being only limited by the bulk resistance it is again the source current that shows the high capacitive peak.

The electrons leave the channel region to both sides but dominantly to the source contact (Figs. 20 and 21). With increasing drain voltage this situation changes after t = 38 ps, when the drain current becomes the slightly higher one (Fig. 20).

4.3 Time constants

Finally it should be mentioned that all time constants are time-dependent. Gate and source currents show the small initial value of $\tau_{S,G} \approx 5$ps which is dramatically increased within the first 10 ps to 20 ps in both the turn-on and the turn-off case. An initial value of $\tau_D = 20$ ps seems to be appropriate for drain current and drain voltage.

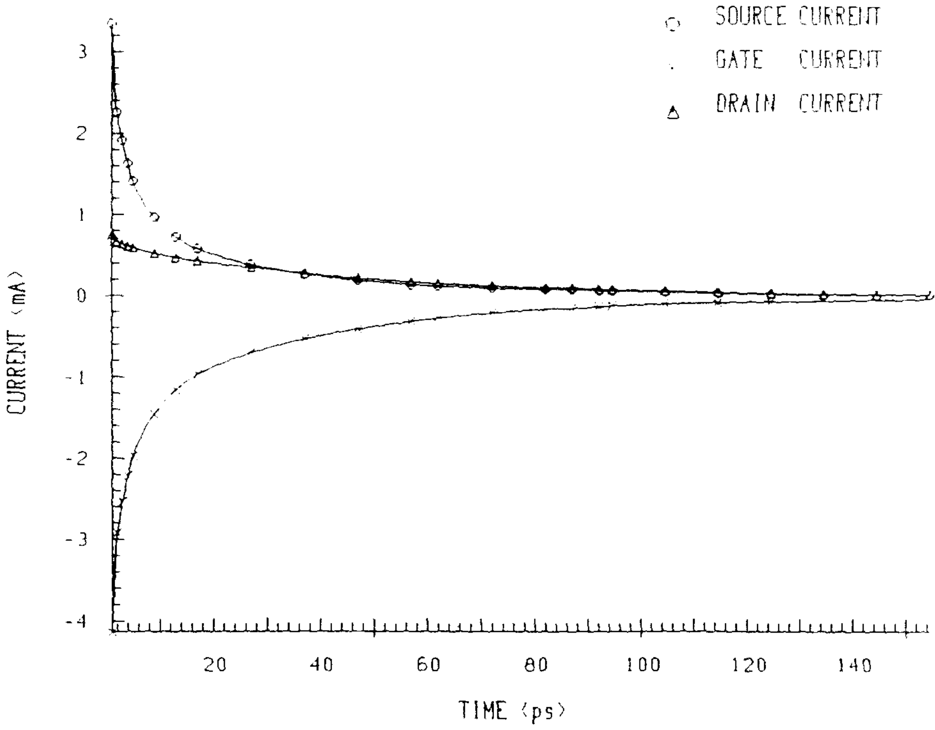

Fig. 20 Contact currents during turn off

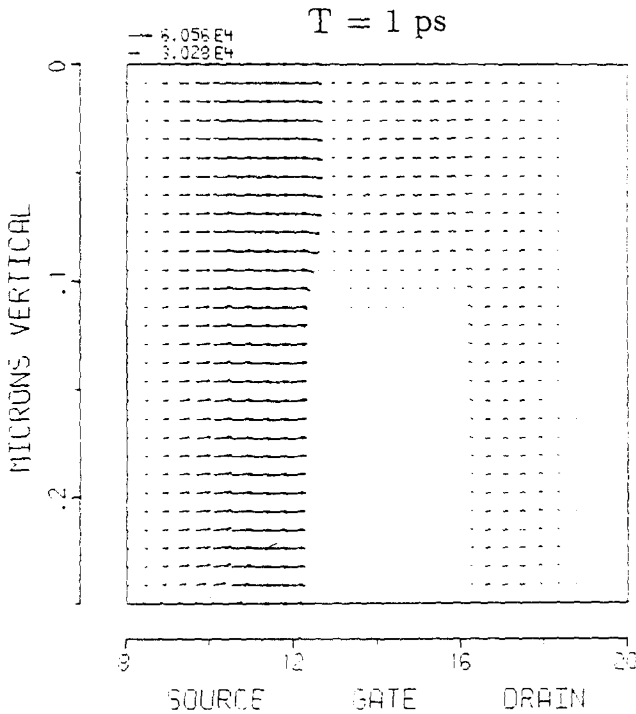

Fig. 21 Direction of the electron current density under the MES gate after 1 ps

5. Acknowledgement

This work was supported by the Siemens AG Research Laboratories, Munich, Germany and by Digital Equipment Corporation, Hudson, U.S.A. and by the 'Fond zur Förderung der wissentschaftlichen Forschung', Project S43/10. The authors would like to thank the 'Interuniversitäre Rechenzentrum' for supplying the large amount of computer resources.

6. References

[1] Houston, T.W., Hite, L.R., Darley, H.M. et al., "Radiation hardness of a silicon MESFET 4Kx1 sRAM", *IEEE Trans. Nucl. Sci.*, NS-31, p. 1483, 1984.
[2] Bohlin, K., and Tove, P.A., "Complementary Si MESFET concept for logic circuits", *Proc. 15th Europ. Solid Dev. Research Conf. ESSDERC 85*, Aachen, p. 230, 1985.
[3] Franz, A.F., Franz, G.A. and Selberherr, S., "BAMBI - a design model for power MOSFETs", *Proc. ICCAD Conf.*, Santa Clara, CA, p. 179, 1984.
[4] Franz, A.F. and Franz, G.A., "BAMBI - a design model for power MOSFETs", *IEEE Trans. CAD*, vol. Cad-4, p. 177, 1985.
[5] Sze, S.M., "Basic equations for semiconductor - device operation", *Physics of Semiconductor Devices*, 2nd edn., Wiley, New York, p. 50, 1981.
[6] Franz, A.F., Franz, G.A., Selberherr, S., Ringhofer, Ch. and Markowich, P., "Finite boxes - a generalization of the finite-differences method suitable for semiconductor device simulation", *IEEE Trans. Electron Devices.*, vol. ED-30, p. 1070, 1983.
[7] Scharfetter, D.L. and Gummel, H.K., "Large-signal analysis of a silicon read diode oscillator", *IEEE Trans. Electron Devices.*, vol. ED-16, p. 64, 1969.
[8] Crowell, C.R. and Sze, S.M., "Current transport in medal-semiconductor barriers", *Solid-State Electronics*, vol. 9, p. 1035, 1965.
[9] Crowell, C.R. and Beguwala, M., "Recombination velocity effects on current diffusion and imref in Schottky barriers", *Solid-State Electronics*, vol. 14, p. 1149, 1971.
[10] Adams, J. and Tang, T., "A revised boundary condition for the numerical analysis of Schottky barrier diodes", *IEEE Electron Device Lett.*, vol. EDL-7, p. 525. 1986.
[11] Stratton, R., "Diffusion of hot and cold electrons in semiconductor barriers", *Phys. Rev.*, vol. 126, p. 2002, 1962.